AIP | The Journal of Chemical Physics

Plasmon transmission through excitonic subwavelength gaps

Maxim Sukharev and Abraham Nitzan

Citation: The Journal of Chemical Physics **144**, 144703 (2016); doi: 10.1063/1.4945446
View online: http://dx.doi.org/10.1063/1.4945446
View Table of Contents: http://scitation.aip.org/content/aip/journal/jcp/144/14?ver=pdfcov
Published by the AIP Publishing

Plasmon transmission through excitonic subwavelength gaps

Maxim Sukharev[1,a)] and Abraham Nitzan[2,3,b)]
[1]*Science and Mathematics Faculty, College of Letters and Sciences, Arizona State University, Mesa, Arizona 85212, USA*
[2]*School of Chemistry, Tel Aviv University, Tel Aviv 69978, Israel*
[3]*Department of Chemistry, University of Pennsylvania, Philadelphia, Pennsylvania 19104, USA*

(Received 28 January 2016; accepted 24 March 2016; published online 12 April 2016)

We study the transfer of electromagnetic energy across a subwavelength gap separating two co-axial metal nanorods. In the absence of spacer in the gap separating the rods, the system exhibits strong coupling behavior between longitudinal plasmons in the two rods. The nature and magnitude of this coupling are studied by varying various geometrical parameters. As a function of frequency, the transmission is dominated by a split longitudinal plasmon peak. The two hybrid modes are the dipole-like "bonding" mode characterized by a peak intensity in the gap and a quadrupole-like "antibonding" mode whose amplitude vanishes at the gap center. When the length of one rod is varied, this mode spectrum exhibits the familiar anti-crossing behavior that depends on the coupling strength determined by the gap width. When off-resonant 2-level emitters are placed in the gap, almost no effect on the frequency dependent transmission is observed. In contrast, when the molecular system is resonant with the plasmonic line shape, the transmission is strongly modified, showing characteristics of strong exciton-plasmon coupling. Most strongly modified is the transmission near the lower frequency "bonding" plasmon mode. The presence of resonant molecules in the gap affects not only the molecule-field interaction but also the spatial distribution of the field intensity and the electromagnetic energy flux across the junction. © *2016 AIP Publishing LLC.* [http://dx.doi.org/10.1063/1.4945446]

I. INTRODUCTION

Studies aimed at understanding the consequences of the interaction of electromagnetic (EM) fields with metal, semiconductor, and molecular nanostructures are done with the aim to construct, characterize, manipulate, and control plasmonic devices.[1] Recurring themes in these studies are the plasmonic response of aggregates of nano-particles[2–30] and the possibility to transmit electromagnetic energy over constrictions substantially smaller than the radiation wavelength.[31] Composite structures (metal-dielectric and metal-semiconductor) are often found useful because light can localize at their interfaces. Of particular importance are metal-molecule composites, where strong plasmon-exciton coupling together with the nonlinear optical response of the molecular system can generate new physical behavior on one hand and provide more control capabilities by tuning the molecular subsystem on the other.

In this paper, we study a class of systems of the latter kind, focusing on the light transmission properties of a model system comprising metal rods and molecular aggregates of sub-wavelength dimensions. Transmission properties of nano-size structure are usually discussed in two connotations. First, following early studies by Gersten and Nitzan,[32,33] there is substantial interest in the way plasmonic particles affect excitation energy transfer in molecular systems.[34–55] Second, plasmonic structure can operate as sub-wavelength waveguides, which are important in the construction of light controlled nano-devices and nano-size optical communication and information storage systems.[56–67] For the latter systems, two principal design concepts have been studied: one comprises a chain of nanoparticles,[61,64] where waveguiding is achieved by plasmon-hopping between nanoparticles and energy transport may be regarded as motion along a plasmonic band; the other uses the optical properties of metal-dielectric (including metal-vacuum) interfaces.[56,59,61–63] Molecular aggregates were used in both design types. In Refs. 57, 64, and 65, they are used as reporters for the distribution of electromagnetic energy along the waveguide, while in Refs. 60, 62, 63, and 67, they constitute an active constituent of the dielectric subsystem. Another way in which a molecular component can affect the operation in devices based on plasmon hybridization and hopping is in affecting the hybridization characteristics of the system. Obviously, the interactions between plasmonic excitations on different particles will depend on the molecular environment between them.[68,69] In the linear response regime and in particular when the molecular optical response is far from resonance with the relevant plasmonic frequencies, this dependence may be accounted for by incorporating a host medium with a suitable frequency dependent dielectric function. This can be done also for a molecular system in resonance with the plasmonic spectrum; however, such a procedure may not properly account for the distinction between lifetime and dephasing relaxation processes. Alternatively, the molecular subsystem is described here explicitly and quantum mechanically using a variant of the procedure described in Ref. 70 (see also Refs. 71–78). This makes it possible to address the regime of *strong exciton-plasmon coupling*,[79] where the molecular species not only

a)Electronic mail: maxim.sukharev@asu.edu
b)Electronic mail: anitzan@upenn.edu

does modify the plasmon-plasmon coupling but also becomes an active component of the transmitting system. We note in passing that this procedure can also describe the molecular system in the non-linear response regime,[80–83] although we do not address this regime in the present study.

The effect of strong exciton-plasmon coupling on the optical response properties of metal-molecules composites has been under active study for some time.[84] Here we focus on its manifestation in the electromagnetic energy-transmission properties of a system comprising two metal cylinders aligned along a common axis with a gap of variable length between them. Light is injected into the system using a source point dipole located at one end of the two metal-rod system, and the transmitted intensity is recorded at the other end. The effect of a molecular aggregate filling the gap between the metal cylinders is studied in order to elucidate the role of several key parameters that characterize the molecular species: (a) molecular density, (b) molecular transition frequency, and (c) molecular lifetime and dephasing relaxation rates. We note that some issues related to this study were addressed in previous works. On the experimental side, Benner *et al.*[85,86] have studied plasmon transmission (and electronic conduction) across small constrictions between metal wires, highlighting the need to account for heating and thermal expansion effects in realistic experiments. In a theoretical study, Neuhauser and co-workers[68,69] have placed a single molecule between two metal spheres in order to simulate its effect on the plasmon-plasmon coupling. While their single molecule model uses a density matrix description that can study the role of molecular relaxation processes, these issues were not explicitly addressed in these studies. Our earlier work[70] and a recent work by Sadeghi[87] have addressed the role of molecular dephasing in the coherent response of strongly coupled exciton-plasmon systems. Gu and co-workers[66] have recently considered the transmission of electromagnetic signal across a gap in a configuration similar to the one studied here, however, without molecules. The present study is aimed to elucidate the way such transmitted energy is affected by strong exciton-plasmon coupling.

II. MODEL

Our system consists of two metal cylinders of lengths L_1 and L_2 and equal diameters D, lying along a common axis and separated by a gap of width ΔL (see the inset of Fig. 1). This gap can be bridged by a molecular aggregate of the same diameter—an assembly of two-level point objects whose optical response is described by the optical Bloch equations.[70] For comparison, we also consider the corresponding system with a vacuum gap and the system with no gap ($\Delta L = 0$, i.e., a single cylinder).

The dynamics of the electric, $\vec{E}$, and magnetic, $\vec{H}$, fields is simulated using classical Maxwell's equations

$$\mu_0 \frac{\partial \vec{H}}{\partial t} = -\nabla \times \vec{E}, \tag{1a}$$

$$\varepsilon_0 \frac{\partial \vec{E}}{\partial t} = \nabla \times \vec{H} - \vec{J}, \tag{1b}$$

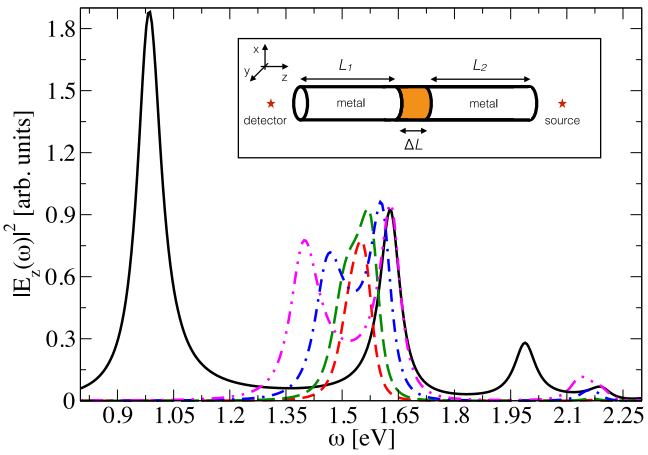

FIG. 1. The inset schematically depicts two closely spaced wires with lengths $L_{1,2}$ separated by a subwavelength gap ΔL. The excitation and detection are carried out locally at a distance of 5 nm from the wires' surface with the source dipole oscillating in the z direction. All simulations in this paper are carried out for wires with a circular cross section of 20 nm in diameter. The main panel shows the transmitted intensity in the longitudinal direction, $|E_z(\omega)|^2$, as a function of the incident frequency. The black line shows the transmitted signal for a single wire with $L_1 = 210$ nm. Other lines are calculated for two closely space identical wires with $L_1 = L_2 = 100$ nm and an empty gap of 60 nm (red short dashed line), 40 nm (green long dashed line), 20 nm (blue dashed-dotted line), and 10 nm (magenta dashed-dotted-dotted line).

where ε_0 and μ_0 are the permittivity and the permeability of free space, respectively. The current source in the Ampere law (1b), $\vec{J}$, corresponds to either the current density in spatial regions occupied by metal (Eq. (3) below) or the macroscopic polarization current, $\vec{J} = \frac{\partial \vec{P}}{\partial t}$, in space filled with a molecular aggregate.

The dispersion of metal is taken into account via Drude model with the dielectric constant of metal, $\varepsilon(\omega)$, in the form

$$\varepsilon(\omega) = \varepsilon_r - \frac{\omega_p^2}{\omega^2 - i\Gamma\omega}, \tag{2}$$

where Γ is the damping parameter, ω_p is the bulk plasma frequency, and ε_r is the high-frequency limit of the dielectric constant. For the range of frequencies considered in this work, the following set of parameters was chosen to represent gold: $\varepsilon_r = 9.5$, $\omega_p = 8.95$ eV, and $\Gamma = 0.069$ eV.[88] We follow the auxiliary differential equation method in order to take into account dispersion (2) in time domain. The corresponding current density in the metal region is evaluated according to the following equation:[89]

$$\frac{\partial \vec{J}}{\partial t} + \Gamma \vec{J} = \varepsilon_0 \omega_p^2 \vec{E}. \tag{3}$$

The optical response of the molecular subsystem is simulated using rate equations for a two-level system driven by a local electric field $\vec{E}$,[90]

$$\frac{dn_1}{dt} - \gamma_{21} n_2 = -\frac{1}{\hbar\Omega_0} \vec{E} \cdot \frac{\partial \vec{P}}{\partial t}, \tag{4a}$$

$$\frac{dn_2}{dt} + \gamma_{21} n_2 = \frac{1}{\hbar\Omega_0} \vec{E} \cdot \frac{\partial \vec{P}}{\partial t}, \tag{4b}$$

$$\frac{\partial^2 \vec{P}}{\partial t^2} + (\gamma_{21} + 2\gamma_d) \frac{\partial \vec{P}}{\partial t} + \Omega_0^2 \vec{P} = -\kappa(n_2 - n_1)\vec{E}, \tag{4c}$$

where n_1 and n_2 ($n_1 + n_2 = n_0$, where n_0 is the number density of molecules) correspond to the populations of the ground and the excited molecular states, respectively, $\vec{P}$ is the macroscopic polarization, γ_{21} is the spontaneous radiative-radiationless decay rate of the excited state,[91] γ_d is the pure dephasing rate, and $\hbar\Omega_0$ is the energy separation of the molecular levels. The coupling constant κ is given by[92]

$$\kappa = \frac{2\Omega_0\mu_{12}^2}{3\hbar}, \tag{5}$$

where μ_{12} is the transition dipole moment. Eqs. (4) and (5) assume that the molecular optical response is isotropic. Consequently, the orientation of the local induced polarization is along the polarization of the local electric field. In the standard situation where the individual molecule does not respond isotropically, the results reported below correspond to the assumption that the distribution of molecular orientations is isotropic. This aspect of the model can be generalized in order to investigate the interesting possibility that molecular effects in plasmon transport can be affected by the molecular orientation. In this work, we do not consider such effects.

The system of coupled equations (1), (3), and (4) is solved numerically on a multi-processor computer.[70] The space is discretized in accordance with finite-difference time domain (FDTD) algorithm[93] in three dimensions. The spatial resolution of $\delta x = \delta y = \delta z = 1$ nm is chosen to achieve numerical convergence and avoid staircase effects (artificial "*hot*" spots in the local field due to discretization of curved surfaces in Cartesian coordinates). The time step used in our simulations is $\delta t = \delta x/(2c) = 1.7$ as, where c is the speed of light in vacuum. Open boundaries are simulated using convolutional perfectly matched layers (CPMLs).[94] We found that for a system considered here the best results were achieved with 19 CPMLs. The total simulation domain for all calculations is $181 \times 181 \times 321$.

We employ short-pulse method (SPM)[70] to calculate linear response of the plasmonic/excitonic system. The time envelope of the probe incident pulse, $f(t)$, is taken in the form of the Blackman-Harris window

$$f(t \le \tau) = \sum_{n=0}^{3} a_n \cos\left(\frac{2\pi n t}{\tau}\right). \tag{6}$$

The pulse duration is denoted as τ, and other parameters are $a_0 = 0.3532$, $a_1 = -0.488$, $a_2 = 0.145$, and $a_3 = -0.0102$. The results discussed in Sec. III are obtained for $\tau = 0.36$ fs pulse duration, leading to an incident pulse with nearly flat spectrum for frequencies between 1 eV and 2 eV.

Unless otherwise stated, for the calculations reported below, we employ two cylindrical identical metal wires with dimensions $L_1 = L_2 = 100$ nm and $D = 20$ nm with a small gap in between. The system is excited locally by a pointwise soft source (classical point dipole) of the functional form given by Eq. (6) that is placed 5 nm from the rightmost wire. Simulations with the driving dipole directed along the z-axis result in significantly higher transmission compared to any transverse polarization and we have therefore used this driving polarization. The transmitted intensity in the z direction, $|E_z|^2$, is detected on the opposite side also at a distance of 5 nm from the leftmost wire at a given point on the grid. It should be noted that the utilization of SPM implies that we consider only elastic scattering. For a case of interacting wires without molecules, it is obviously the case as the optical response of metal is treated linearly using Drude model. In case of molecules, one has to keep the incident peak amplitude low enough such that the population of the molecular excited state is always significantly smaller than 1. In the simulations discussed below, this condition was carefully monitored at all times.

III. RESULTS AND DISCUSSION

The structure composed of two closely spaced wires shown in the inset of Fig. 1 is examined first with an empty gap between the wires. A single wire exhibits two kinds of surface plasmon-polariton (SPP) modes: longitudinal mode associated with oscillations of the charge density along the z-axis and transverse mode corresponding to oscillations in the direction perpendicular to z-axis.[95]

Consider first the transmission characteristics of a single wire ($L_1 = 210$ nm). In the spectral regime displayed, three peaks are shown. By examining their wire-length dependence and the corresponding charge densities,[95] the lower frequency peak at $\omega = 0.98$ eV is identified as a longitudinal dipolar plasmon, and the next one at 1.64 eV is found to be a longitudinal quadrupole plasmon while the peak at 2.1 eV corresponds to the transverse dipolar plasmon. For a single wire of length 100 nm, the longitudinal dipole mode peaks at 1.54 eV, and the longitudinal quadrupolar mode has moved to higher frequency above the range shown, while the transverse mode remains at 2.1 eV.

With a small gap separating the two wires, one can expect to see a manifestation of the interaction between two longitudinal SPP modes supported by each wire. As two identical wires support modes with the same frequency, the close proximity of such modes permits the energy exchange between wires and thus lifts the degeneracy. This effect is clearly seen in Fig. 1 as a splitting of the longitudinal SPP mode at 1.54 eV. The splitting is barely noticeable for a gap of 60 nm since SPP modes are evanescent and decay exponentially with a distance from the surface of each wire, the gap becomes narrower as the splitting significantly increases reaching 232 meV for a 10 nm gap. This Rabi splitting is manifestation of the strong coupling between SPPs[79] that permit efficient energy exchange between wires.[84] By comparing transmission through a single wire (black solid line) and through two closely spaced wires with a gap of 10 nm (magenta dashed-dotted-dotted line), we observe nearly perfect overlap of the quadrupole mode for a single wire with the high frequency mode in the system of coupled wires. Similar simulations comparing transmission through wider gaps with that through a single wire with a corresponding length confirm the quadrupole nature of the high frequency mode.

Finally, we note that the transmission in vacuum if wires are removed is several orders of magnitude smaller than that shown in Fig. 1. Exciting plasmon resonances in the wire(s) clearly increases and focuses transmission in the wire direction.

To further scrutinize the strong coupling between interacting longitudinal SPP modes, we perform a series

of simulations varying the length of one wire while keeping the length of the other constant. This allows us to alter the frequency of one of the longitudinal SPP resonances sweeping through the other. The results of the simulations are shown in Fig. 2. We note that the high energy SPP mode seen in Fig. 2(a) at 2.16 eV is the transverse SPP resonance position changing mildly from 2.15 eV to 2.2 eV when the length of one of the wires varies. The structure of the splitting of the longitudinal mode spectrum changes significantly, with the higher frequency peak changing much faster than the lower one. This apparent asymmetry is easily explained by referring to the avoided crossing behavior shown in Fig. 2(b): when the length of the wire is comparable to its diameter, it scatters light as a nanoparticle with a single dipolar Mie resonance of frequency similar to the transverse mode (2.16 eV). As the length increases, this mode moves to the red while the unperturbed mode of the other wire of fixed length is unchanged. An avoided crossing is seen when the two lengths match.

Several other observations can be made. First, although the transversal modes of the two wires are in principle also coupled, this coupling is too weak to give a noticeable Rabi splitting. Second, even at the shortest length similar to the diameter, the plasmon frequency associated with the short wire is affected by the presence of the other wire and slightly deviates from the value obtained for the isolated wire (green dashed-dotted line in Fig. 2(b)). This probably results from the damping and frequency shift affected by the proximity to a dissipative dielectric object (the second wire) but may also reflect the effect of interaction with the transversal plasmon of this second wire. As expected, similar results were obtained when we varied L_2 with L_1 being kept constant.

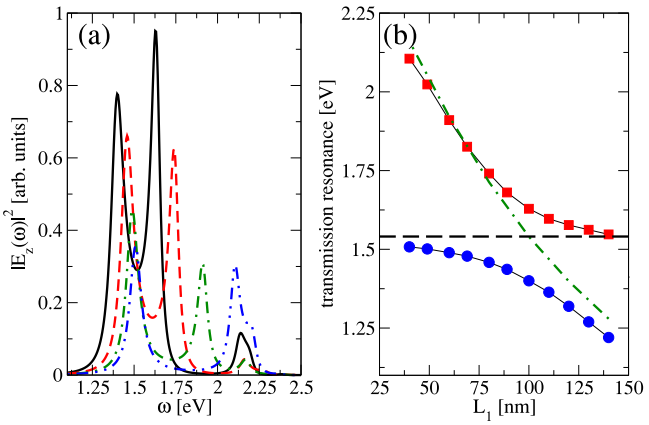

FIG. 2. Panel (a) shows the transmitted intensity in the longitudinal direction, $|E_z(\omega)|^2$, as a function of the incident frequency, for the system of two wires with the fixed $L_2 = 100$ nm and variable L_1 and a gap of $\Delta L = 10$ nm between the wires (see the inset of Fig. 1 for details of the geometry). The black solid line shows results for symmetric system with $L_1 = 100$ nm, red dashed line shows data for $L_1 = 80$ nm, green dashed-dotted line shows results for $L_1 = 60$ nm, and blue dashed-dotted-dotted line shows results for $L_1 = 40$ nm. The peak at 2.15 eV corresponds to the transversal mode of these wires and is only affected by wire's length. Panel (b) shows the energies of two transmission resonances as functions of the wire's length L_1. Horizontal black dashed line indicates the energy of the longitudinal SPP resonance for a single 100 nm wire. Green dashed-dotted line shows how the energy of the longitudinal SPP resonance of a single wire varies with its length. Other parameters are the same as in Fig. 1.

Finally we note that these observations may be sensitive to the polarization of the injecting source. We defer the study of this issue to later work.

In order to understand the physics behind the Rabi splitting, we examine spatial distributions of the electromagnetic energy at two resonant frequencies. In the strong coupling regime, the system of two wires forms two states as illustrated in Fig. 3. The low energy mode has a maximum in the gap while the high energy mode has a node. Obviously we are seeing the equivalent of the behavior of bonding and antibonding orbitals in a system of two coupled emitters[27] as this was confirmed in Fig. 1 by comparing transmission through a single wire with that through two closely spaced wires.

Next we add a molecular aggregate filling the gap between the interacting wires and investigate how molecules resonant to longitudinal SPP modes modify the transmission spectrum. The values of the molecular parameters used in this work are the molecular transition dipole $\mu_{12} = 25$ Debye, $\gamma_{21} = 6.892 \times 10^{-4}$ eV (corresponding to 6 ps), $\gamma_d = 6.565 \times 10^{-3}$ eV (corresponding to 630 fs). When a molecular aggregate is placed inside the gap, the local electromagnetic field is coupled to the molecules. This system is analogous to three coupled oscillators: two longitudinal SPP electromagnetic modes and molecular excitons. The ratio between the intensities of the two SPP modes spatially averaged over gap's volume for the parameters in Fig. 3 is 59.95. The coupling between each SPP mode and the molecular exciton depends on the corresponding local electric field amplitude in the gap. One can therefore anticipate that the low energy plasmon mode with a higher amplitude in the gap would couple to molecules appreciably more stronger than the high frequency mode. As noted above, the high frequency mode is the antibonding mode with a node in the gap, which in frequency to the quadrupolar mode of a single wire of similar total length. Its low intensity in the gap reflects this antibonding nature.

Fig. 4 shows results of simulations with varying molecular transition energy, Ω_0. When Ω_0 is close to the low energy mode, the transmission exhibits three resonances with actual transmission dropping by more than 2 orders of magnitude for the incident photon energy slightly higher than the molecular transition (black solid line, Fig. 4(a), $\omega_{inc} = 1.432$ eV). Additional simulations (not shown) were carried out to calculate a spatial distribution of the electromagnetic energy for parameters corresponding to very low transmission. We found that in this case, the molecular aggregate acts as a very efficient absorber dropping the overall transmission. When the molecular transition energy is around 1.54 eV, the transmission exhibits signs of interference effects as its shape has a clear Fano line shape (green dashed-dotted line, Fig. 4(a)). However at energies close to the high energy mode near 1.62 eV, the transmission looks nearly unperturbed compared to the case without molecules.

Fig. 4(b) shows results of the fine sweep over the molecular transition frequency, Ω_0. Since the molecular aggregate is placed in the gap between two wires, one would expect to observe coupling between the low frequency SPP mode (mainly localized in the gap) and nearly no effect on the antibonding mode. Such a regime is manifested by a

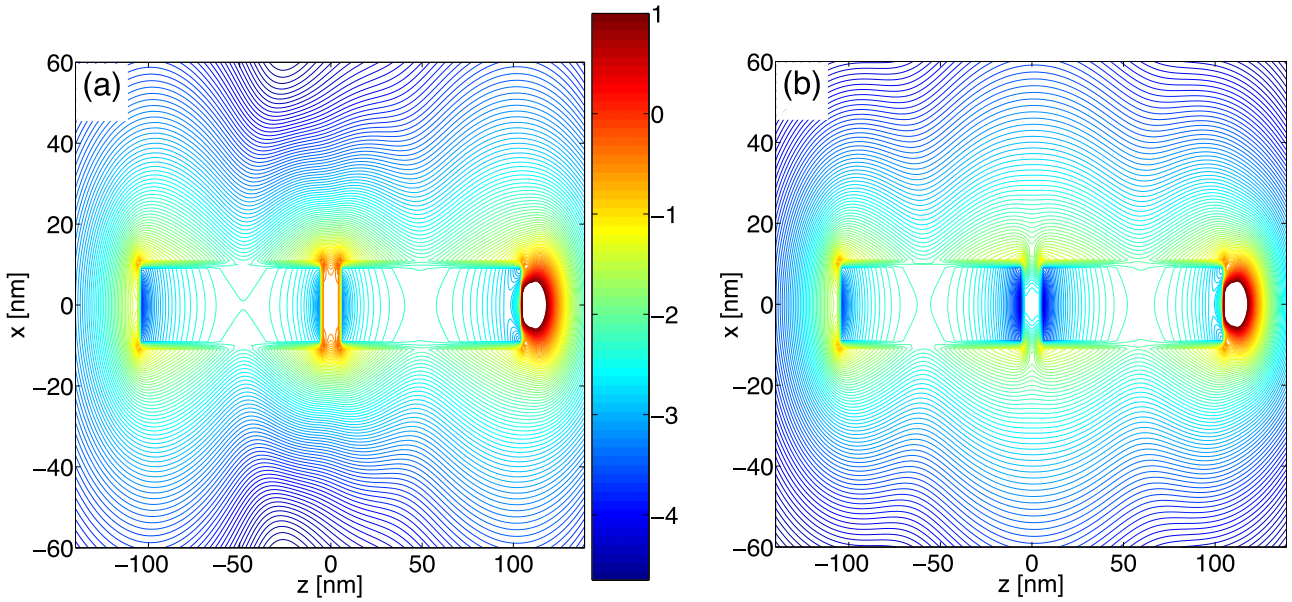

FIG. 3. Steady-state electromagnetic intensity distributions for the system of two interacting wires separated by an empty gap of 10 nm (see the inset in Fig. 1 for details of the geometry). The length of each wire is 100 nm. The system is excited by a pointwise dipole placed at the right side and oscillating in longitudinal z-direction. Panel (a) shows normalized electromagnetic intensity as a function of x and z (in nm) for the incident frequency of 1.40 eV (the low energy resonance for data shown as a magenta dashed-dotted-dotted line in Fig. 1). Panel (b) shows normalized electromagnetic intensity calculated for frequency 1.63 eV (the high energy resonance for data shown as a magenta dashed-dotted-dotted line in Fig. 1). The electromagnetic intensity distributions are plotted in logarithmic scale and normalized to the incident intensity.

clear avoided crossing near 1.4 eV with the Rabi splitting reaching about 150 meV. The effect of resonant molecules on the antibonding mode located near 1.63 eV is not trivial. Although there no strong coupling behavior is observed, the molecules act as absorbers resulting in a narrow minimum occurring inside the transmission maximum (see blue dashed-dotted-dotted line in Fig. 4(a)).

To investigate how electromagnetic energy is transported through a system of closely spaced nanowires, we performed a series of simulations varying the physical environment of the gap. One set of simulations was carried out with non-resonant molecules filling the gap. We found that there is almost no effect on the transmission if the molecular transition energy is below 1.2 eV irrespective of how high the molecular concentration is. This suggested another test, namely, to replace the molecules with a perfect electric conductor (PEC) completely closing the gap between the wires. Simulations showed that the effect of PEC on transmission is a red-shift of the low energy mode while the energy of the "antibonding" state remains constant. For the system with $\Delta L = 10$ nm and $L_1 = L_2 = 100$ nm, the shift of the low energy mode is 0.4 eV. These findings indicate that the electromagnetic energy transport occurs primarily along the surface of wires. Additional simulations examining the spatial distributions of

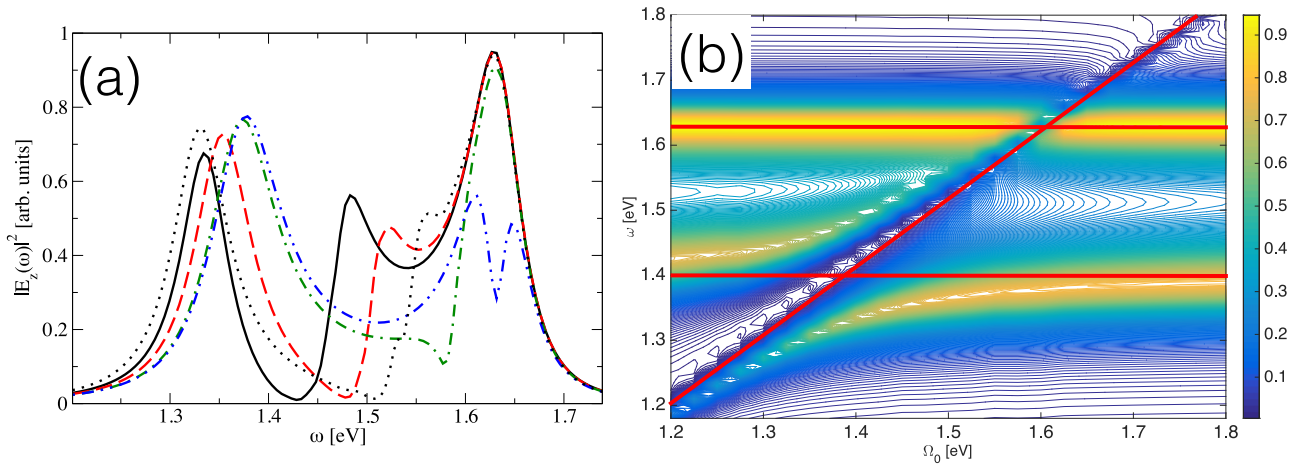

FIG. 4. Coupled plasmon-exciton system. Panel (a) shows the transmission as a function of the incident frequency calculated for two wires with a length of $L_1 = L_2 = 100$ nm with a molecular aggregate placed in the gap between the wires ($\Delta L = 10$ wide). The molecular transition frequency $\Omega_0 = 1.40$ eV corresponds to the solid and dotted black lines (see below), dashed red line shows data for $\Omega_0 = 1.45$ eV, dashed-dotted green line shows results for $\Omega_0 = 1.55$ eV, and dashed-dotted-dotted blue line shows data for $\Omega_0 = 1.60$ eV. The molecular number density is 5×10^{25} m^{-3} for all lines except for the dotted black line, which is calculated at 10^{26} m^{-3}. Panel (b) shows transmission as a function of the incident frequency and the molecular transition frequency, Ω_0. Two horizontal red lines show the energies of the hybrid SP modes without molecules in the gap. The third red line with a slope shows the molecular transition frequency sweep.

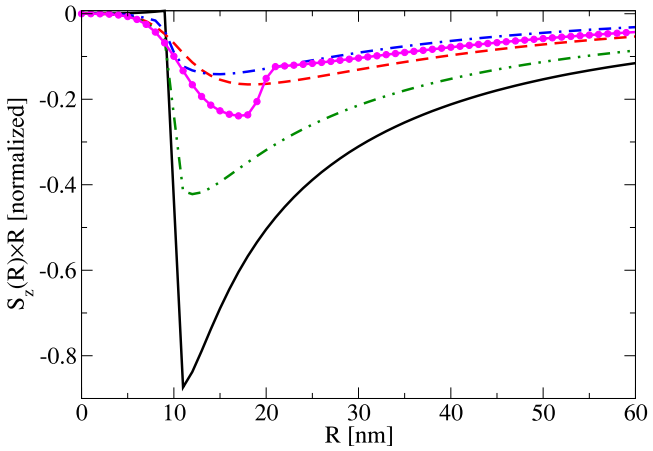

FIG. 5. The z-component of the Poynting vector calculated at the center of the system (middle of the gap) and at distance R from the axis connecting wires, multiplied by this distance R, $S_z \times R$, as a function of R. The black solid line shows results for a single wire 210 nm long calculated at $\omega = 0.984$ eV (see black line in Fig. 1). The red dashed line presents results for two coaxial wires with $L_1 = L_2 = 100$ nm and an empty gap of $\Delta L = 10$ nm calculated at $\omega = 1.4$ eV (see magenta dashed-dotted-dotted line in Fig. 1). The green dashed-dotted-dotted line shows results for two wires with the same characteristics as for the red line but with a gap filled with a non-dispersive dielectric with $\varepsilon = 5$ calculated at $\omega = 1.24$ eV (which corresponds to the maximum transmission). The blue dashed-dotted line shows results for the same system of two wires with the gap filled with molecules. The latter is calculated at $\omega = 1.33$ eV (see black solid line in Fig. 4(a)). The magenta line connecting circles shows results for two coaxial wires with $L_1 = L_2 = 100$ nm separated by a gap of $\Delta L = 10$ nm submerged in molecular cylinder (radius 10 nm and length 210 nm). It is calculated at $\omega = 1.58$ eV, which is the position of the largest polariton peak seen in the transmission spectrum of this system. The molecular transition frequency in all calculations is $\Omega_0 = 1.4$ eV and $n_0 = 5 \times 10^{25}$ m^{-3}. All wires are 20 nm in diameter.

the Poynting vector confirmed that hypothesis as illustrated in Fig. 5. The z-component of the Poynting vector, $S_z(R)$, is evaluated for several representative cases, and $S_z(R) \times R$ is plotted as a function of the radial distance from the symmetry axis connecting two wires. We note that the negative sign of the energy flux corresponds to the propagation of EM energy from the source towards the detector (see the inset in Fig. 1). The magenta line shows simulations performed for a system comprised of two wires fully submerged in a cylinder composed of molecules. This system exhibit several resonances in the transmission spectrum (not shown). The "bonding" mode (see Fig. 1, blue dashed-dotted line, resonance at 1.6 eV, see also Fig. 3(b)) splits into two modes due to strong coupling between molecules and the plasmon mode. The frequency at which the energy flux is evaluated corresponds to the maximum transmission at 1.58 eV. One can clearly see the EM energy mostly localized in the molecular layer $10\,\text{nm} < R < 20\,\text{nm}$. All five cases clearly demonstrate the fact that the propagation mainly occurs along the surface of wires.

Finally, the following observation from our simulation may appear surprising: the result shown in Fig. 4 is not sensitive to the nature of the relaxation processes modeled in Eq. (4) in the following sense: If the magnitudes of the population and dephasing relaxation rates are varied such that $\gamma_{21} + 2\gamma_d = \text{constant}$, the same spectrum is produced. This behavior characterizes systems in which spontaneous emission does not play a significant part in the spectral response (in the present calculation using classical EM field, it is simply ignored). In such systems, the optical response is dominated by the classical molecular polarization, which is sensitive only to the sum $\gamma_{21} + 2\gamma_d$.

IV. CONCLUSION

Using a numerical scheme based on the coupled Maxwell-Bloch equations implemented within the FDTD electromagnetic numerical solver, we have studied the transfer of electromagnetic radiation across a molecular gap separating two co-axial metal cylinders. In the absence of the molecular spacer in the gap separating the rods, this system exhibits the consequence of plasmon-plasmon coupling, in particular between longitudinal plasmons in the two rods. The nature and magnitude of this coupling can be studied by varying the gap width as well as by changing the length of one wire keeping the other fixed, which produces the familiar non-crossing behavior. As a function of frequency, the transmission is dominated by a split longitudinal plasmon peak. The two hybrid modes are the dipole-like "bonding" mode characterized by a peak intensity in the gap, and a quadrupole-like "antibonding" mode whose amplitude vanishes at the gap center.

When off-resonant 2-level molecules are placed in the gap, almost no effect on the frequency dependent transmission is observed. We have traced this behavior to the observation that much of the transmission takes place along the cylinders' edge. The "bonding" mode is significantly affected by the dielectric properties of the gap. In contrast, when the molecular system is in resonance with the plasmonic line shape, the transmission is strongly modified, showing characteristics of strong exciton-plasmon coupling, modifying mostly the transmission near the lower frequency "bonding" plasmon mode. It is interesting to note that the presence of resonant molecules species in the gap affects not only the molecule-field interaction but also the spatial distribution of the field intensity and the electromagnetic energy flux across the junction.

This study can be extended in several ways. First and obvious is the fact that the observation reported here can be sensitive to the molecular orientation in the gap. In the present study, we have assumed that this orientation is random, implying an average isotropic molecular response, and a preferred molecular orientation may be an important parameter in determining the transmission across the junction. A more subtle issue is the role played by molecular fluorescence. In present experimental studies, the fluorescence signal from dye molecules placed along the nanowaveguide is used to report on the electromagnetic field distribution along the guide.[64,65] In the configuration used in the present study, spontaneous emission by strongly fluorescent molecule may play an active role in the observed optical response. To study such an effect, one needs to go beyond the current level of description that treats the electromagnetic field completely classically. We defer such considerations to future work.

ACKNOWLEDGMENTS

Both authors acknowledge support by the collaborative BSF Grant No. 2014113. M.S. is also grateful for financial

support by AFOSR Grant No. FA9550-15-1-0189. The research of A.N. is also supported by the Israel Science Foundation.

[1]A. A. Maradudin, J. R. Sambles, and W. L. Barnes, *Modern Plasmonics* (Elsevier, 2014), Vol. 4.
[2]B. Nikoobakht and M. A. El-Sayed, "Surface-enhanced Raman scattering studies on aggregated gold nanorods," J. Phys. Chem. A **107**, 3372–3378 (2003).
[3]G. Gantzounis, N. Stefanou, and V. Yannopapas, "Optical properties of a periodic monolayer of metallic nanospheres on a dielectric waveguide," J. Phys.: Condens. Matter **17**, 1791 (2005).
[4]C. E. Talley, J. B. Jackson, C. Oubre, N. K. Grady, C. W. Hollars, S. M. Lane, T. R. Huser, P. Nordlander, and N. J. Halas, "Surface-enhanced Raman scattering from individual Au nanoparticles and nanoparticle dimer substrates," Nano Lett. **5**, 1569–1574 (2005).
[5]K. Imura, H. Okamoto, M. K. Hossain, and M. Kitajima, "Near-field imaging of surface-enhanced Raman active sites in aggregated gold nanoparticles," Chem. Lett. **35**, 78–79 (2006).
[6]P. K. Jain, S. Eustis, and M. A. El-Sayed, "Plasmon coupling in nanorod assemblies: Optical absorption, discrete dipole approximation simulation, and exciton-coupling model," J. Phys. Chem. B **110**, 18243–18253 (2006).
[7]P. K. Jain, W. Huang, and M. A. El-Sayed, "On the universal scaling behavior of the distance decay of plasmon coupling in metal nanoparticle pairs: A plasmon ruler equation," Nano Lett. **7**, 2080–2088 (2007).
[8]V. Yannopapas and N. V. Vitanov, "Spontaneous emission of a two-level atom placed within clusters of metallic nanoparticles," J. Phys.: Condens. Matter **19**, 096210 (2007).
[9]P. K. Jain and M. A. El-Sayed, "Surface plasmon coupling and its universal size scaling in metal nanostructures of complex geometry: Elongated particle pairs and nanosphere trimers," J. Phys. Chem. C **112**, 4954–4960 (2008).
[10]W. Li, P. H. C. Camargo, X. Lu, and Y. Xia, "Dimers of silver nanospheres: Facile synthesis and their use as hot spots for surface-enhanced Raman scattering," Nano Lett. **9**, 485–490 (2009).
[11]M. Chergui, A. Melikyan, and H. Minassian, "Calculation of surface plasmon frequencies of two, three, and four strongly interacting nanospheres," J. Phys. Chem. C **113**, 6463–6471 (2009).
[12]V. D. Miljković, T. Pakizeh, B. Sepulveda, P. Johansson, and M. Käll, "Optical forces in plasmonic nanoparticle dimers," J. Phys. Chem. C **114**, 7472–7479 (2010).
[13]K. L. Wustholz, A.-I. Henry, J. M. McMahon, R. G. Freeman, N. Valley, M. E. Piotti, M. J. Natan, G. C. Schatz, and R. P. V. Duyne, "Structure-activity relationships in gold nanoparticle dimers and trimers for surface-enhanced Raman spectroscopy," J. Am. Chem. Soc. **132**, 10903–10910 (2010).
[14]C. Farcau and S. Astilean, "Mapping the SERS efficiency and hot-spots localization on gold film over nanospheres substrates," J. Phys. Chem. C **114**, 11717–11722 (2010).
[15]P. A. Letnes, I. Simonsen, and D. L. Mills, "Substrate influence on the plasmonic response of clusters of spherical nanoparticles," Phys. Rev. B **83**, 075426 (2011).
[16]E. R. Encina and E. A. Coronado, "Near field enhancement in Ag Au nanospheres heterodimers," J. Phys. Chem. C **115**, 15908–15914 (2011).
[17]D. Whitmore, P. Z. El-Khoury, L. Fabris, P. Chu, G. C. Bazan, E. O. Potma, and V. A. Apkarian, "High sensitivity surface-enhanced Raman scattering in solution using engineered silver nanosphere dimers," J. Phys. Chem. C **115**, 15900–15907 (2011).
[18]J. Jung, M. L. Trolle, K. Pedersen, and T. G. Pedersen, "Indirect near-field absorption mediated by localized surface plasmons," Phys. Rev. B **84**, 165447 (2011).
[19]M. Banik, A. Nag, P. Z. El-Khoury, A. Rodriguez Perez, N. Guarrotxena, G. C. Bazan, and V. A. Apkarian, "Surface-enhanced Raman scattering of a single nanodumbbell: Dibenzyldithio-linked silver nanospheres," J. Phys. Chem. C **116**, 10415–10423 (2012).
[20]W.-S. Chang, B. Willingham, L. S. Slaughter, S. Dominguez-Medina, P. Swanglap, and S. Link, "Radiative and nonradiative properties of single plasmonic nanoparticles and their assemblies," Acc. Chem. Res. **45**, 1936–1945 (2012).
[21]M. Banik, P. Z. El-Khoury, A. Nag, A. Rodriguez-Perez, N. Guarrottxena, G. C. Bazan, and V. A. Apkarian, "Surface-enhanced Raman trajectories on a nano-dumbbell: Transition from field to charge transfer plasmons as the spheres fuse," ACS Nano **6**, 10343–10354 (2012).
[22]J. C. Fraire, L. A. Pérez, and E. A. Coronado, "Cluster size effects in the surface-enhanced Raman scattering response of Ag and Au nanoparticle aggregates: Experimental and theoretical insight," J. Phys. Chem. C **117**, 23090–23107 (2013).
[23]E. Prodan, C. Radloff, N. J. Halas, and P. Nordlander, "A hybridization model for the plasmon response of complex nanostructures," Science **302**, 419–422 (2003).
[24]P. Nordlander, C. Oubre, E. Prodan, K. Li, and M. I. Stockman, "Plasmon hybridization in nanoparticle dimers," Nano Lett. **4**, 899–903 (2004).
[25]P. Nordlander and E. Prodan, "Plasmon hybridization in nanoparticles near metallic surfaces," Nano Lett. **4**, 2209–2213 (2004).
[26]E. Prodan and P. Nordlander, "Plasmon hybridization in spherical nanoparticles," J. Chem. Phys. **120**, 5444–5454 (2004).
[27]N. J. Halas, S. Lal, W.-S. Chang, S. Link, and P. Nordlander, "Plasmons in strongly coupled metallic nanostructures," Chem. Rev. **111**, 3913–3961 (2011).
[28]R. Esteban, A. G. Borisov, P. Nordlander, and J. Aizpurua, "Bridging quantum and classical plasmonics with a quantum-corrected model," Nat. Commun. **3**, 825 (2012).
[29]A. E. Schlather, N. Large, A. S. Urban, P. Nordlander, and N. J. Halas, "Near-field mediated plexcitonic coupling and giant rabi splitting in individual metallic dimers," Nano Lett. **13**, 3281–3286 (2013).
[30]N. Harris, M. D. Arnold, M. G. Blaber, and M. J. Ford, "Plasmonic resonances of closely coupled gold nanosphere chains," J. Phys. Chem. C **113**, 2784–2791 (2009).
[31]Other important recurring themes such as induction of transient dielectric properties, lifetime of radiative and non-radiative processes, and formation and utilization of hot electrons and local hotspots are not related to the present study.
[32]J. I. Gersten and A. Nitzan, "Accelerated energy transfer between molecules near a solid particle," Chem. Phys. Lett. **104**, 31–37 (1984).
[33]X. M. Hua, J. I. Gersten, and A. Nitzan, "Theory of energy transfer between molecules near solid state particles," J. Chem. Phys. **83**, 3650–3659 (1985).
[34]P. Andrew and W. L. Barnes, "Energy transfer across a metal film mediated by surface plasmon polaritons," Science **306**, 1002–1005 (2004).
[35]J. I. Gersten, "Fluorescence resonance energy transfer near thin films on surfaces," Plasmonics **2**, 65–77 (2007).
[36]J. Zhang, Y. Fu, and J. R. Lakowicz, "Enhanced Förster resonance energy transfer (FRET) on a single metal particle," J. Phys. Chem. C **111**, 50–56 (2007).
[37]F. Reil, U. Hohenester, J. R. Krenn, and A. Leitner, "Förster-type resonant energy transfer influenced by metal nanoparticles," Nano Lett. **8**, 4128–4133 (2008).
[38]C. A. Marocico and J. Knoester, "Intermolecular resonance energy transfer in the presence of a dielectric cylinder," Phys. Rev. A **79**, 053816 (2009).
[39]S. Saini, G. Srinivas, and B. Bagchi, "Distance and orientation dependence of excitation energy transfer: From molecular systems to metal nanoparticles," J. Phys. Chem. B **113**, 1817–1832 (2009).
[40]H. Y. Chung, P. T. Leung, and D. P. Tsai, "Enhanced intermolecular energy transfer in the vicinity of a plasmonic nanorice," Plasmonics **5**, 363–368 (2010).
[41]D. Martín-Cano, L. Martín-Moreno, F. J. García-Vidal, and E. Moreno, "Resonance energy transfer and superradiance mediated by plasmonic nanowaveguides," Nano Lett. **10**, 3129–3134 (2010).
[42]X.-R. Su, W. Zhang, L. Zhou, X.-N. Peng, and Q.-Q. Wang, "Plasmon-enhanced Förster energy transfer between semiconductor quantum dots: Multipole effects," Opt. Express **18**, 6516–6521 (2010).
[43]V. Faessler, C. Hrelescu, A. A. Lutich, L. Osinkina, S. Mayilo, F. Jäckel, and J. Feldmann, "Accelerating fluorescence resonance energy transfer with plasmonic nanoresonators," Chem. Phys. Lett. **508**, 67–70 (2011).
[44]C. A. Marocico and J. Knoester, "Effect of surface-plasmon polaritons on spontaneous emission and intermolecular energy-transfer rates in multilayered geometries," Phys. Rev. A **84**, 053824 (2011).
[45]V. N. Pustovit and T. V. Shahbazyan, "Resonance energy transfer near metal nanostructures mediated by surface plasmons," Phys. Rev. B **83**, 085427 (2011).
[46]M. A. Antón, F. Carreño, S. Melle, O. G. Calderón, E. Cabrera-Granado, J. Cox, and M. R. Singh, "Plasmonic effects in excitonic population transfer in a driven semiconductor–metal nanoparticle hybrid system," Phys. Rev. B **86**, 155305 (2012).
[47]M. Lunz, X. Zhang, V. A. Gerard, Y. K. Gun'ko, V. Lesnyak, N. Gaponik, A. S. Susha, A. L. Rogach, and A. L. Bradley, "Effect of metal nanoparticle concentration on localized surface plasmon mediated Förster resonant energy transfer," J. Phys. Chem. C **116**, 26529–26534 (2012).
[48]L. Zhao, T. Ming, L. Shao, H. Chen, and J. Wang, "Plasmon-controlled Förster resonance energy transfer," J. Phys. Chem. C **116**, 8287–8296 (2012).

[49]A. Angioni, S. Corni, and B. Mennucci, "Can we control the electronic energy transfer in molecular dyads through metal nanoparticles? A QM/continuum investigation," Phys. Chem. Chem. Phys. **15**, 3294–3303 (2013).
[50]V. Karanikolas, C. A. Marocico, and A. L. Bradley, "Spontaneous emission and energy transfer rates near a coated metallic cylinder," Phys. Rev. A **89**, 063817 (2014).
[51]K. F. Chou and A. M. Dennis, "Förster resonance energy transfer between quantum dot donors and quantum dot acceptors," Sensors **15**, 13288–13325 (2015).
[52]C. A. Marocico, X. Zhang, and A. L. Bradley, "A theoretical investigation of the influence of gold nanosphere size on the decay and energy transfer rates and efficiencies of quantum emitters," J. Chem. Phys. **144**, 024108 (2016).
[53]M. G. Kucherenko, V. N. Stepanov, and N. Y. Kruchinin, "Intermolecular nonradiative energy transfer in clusters with plasmonic nanoparticles," Opt. Spectrosc. **118**, 103–110 (2015).
[54]V. N. Pustovit, A. M. Urbas, and T. V. Shahbazyan, "Energy transfer in plasmonic systems," J. Opt. **16**, 114015 (2014).
[55]O. Roslyak, C. Cherqui, D. H. Dunlap, and A. Piryatinski, "Effect of localized surface-plasmon mode on exciton transport and radiation emission in carbon nanotubes," J. Phys. Chem. B **118**, 8070–8080 (2014).
[56]W. L. Barnes, A. Dereux, and T. W. Ebbesen, "Surface plasmon subwavelength optics," Nature **424**, 824–830 (2003).
[57]S. A. Maier, P. G. Kik, H. A. Atwater, S. Meltzer, E. Harel, B. E. Koel, and A. A. G. Requicha, "Local detection of electromagnetic energy transport below the diffraction limit in metal nanoparticle plasmon waveguides," Nat. Mater. **2**, 229–232 (2003).
[58]R. Zia, M. D. Selker, P. B. Catrysse, and M. L. Brongersma, "Geometries and materials for subwavelength surface plasmon modes," J. Opt. Soc. Am. A **21**, 2442–2446 (2004).
[59]R. F. Oulton, V. J. Sorger, D. A. Genov, D. F. P. Pile, and X. Zhang, "A hybrid plasmonic waveguide for subwavelength confinement and long-range propagation," Nat. Photonics **2**, 496–500 (2008).
[60]J. Grandidier, G. C. des Francs, S. Massenot, A. Bouhelier, L. Markey, J.-C. Weeber, C. Finot, and A. Dereux, "Gain-assisted propagation in a plasmonic waveguide at telecom wavelength," Nano Lett. **9**, 2935–2939 (2009).
[61]V. J. Sorger, Z. Ye, R. F. Oulton, Y. Wang, G. Bartal, X. Yin, and X. Zhang, "Experimental demonstration of low-loss optical waveguiding at deep subwavelength scales," Nat. Commun. **2**, 331 (2011).
[62]T. Ellenbogen, P. Steinvurzel, and K. B. Crozier, "Strong coupling between excitons in J-aggregates and waveguide modes in thin polymer films," Appl. Phys. Lett. **98**, 261103 (2011).
[63]T. Ellenbogen and K. B. Crozier, "Exciton-polariton emission from organic semiconductor optical waveguides," Phys. Rev. B **84**, 161304 (2011).
[64]A. Paul, D. Solis, K. Bao, W.-S. Chang, S. Nauert, L. Vidgerman, E. R. Zubarev, P. Nordlander, and S. Link, "Identification of higher order long-propagation-length surface plasmon polariton modes in chemically prepared gold nanowires," ACS Nano **6**, 8105–8113 (2012).
[65]D. Solis, A. Paul, J. Olson, L. S. Slaughter, P. Swanglap, W.-S. Chang, and S. Link, "Turning the corner: Efficient energy transfer in bent plasmonic nanoparticle chain waveguides," Nano Lett. **13**, 4779–4784 (2013).
[66]Z. Gu, S. Liu, S. Sun, K. Wang, Q. Lyu, S. Xiao, and Q. Song, "Photon hopping and nanowire based hybrid plasmonic waveguide and ring-resonator," Sci. Rep. **5**, 9171 (2015).
[67]I. Carmeli, M. Cohen, O. Heifler, Y. Lilach, Z. Zalevsky, V. Mujica, and S. Richter, "Spatial modulation of light transmission through a single microcavity by coupling of photosynthetic complex excitations to surface plasmons," Nat. Commun. **6**, 7334 (2015).
[68]K. Lopata and D. Neuhauser, "Nonlinear nanopolaritonics: Finite-difference time-domain Maxwell–Schrödinger simulation of molecule-assisted plasmon transfer," J. Chem. Phys. **131**, 014701 (2009).
[69]C. Arntsen, K. Lopata, M. R. Wall, L. Bartell, and D. Neuhauser, "Modeling molecular effects on plasmon transport: Silver nanoparticles with tartrazine," J. Chem. Phys. **134**, 084101 (2011).
[70]M. Sukharev and A. Nitzan, "Numerical studies of the interaction of an atomic sample with the electromagnetic field in two dimensions," Phys. Rev. A **84**, 043802 (2011).
[71]R. Bonifacio and L. A. Lugiato, "Cooperative radiation processes in two-level systems: Superfluorescence," Phys. Rev. A **11**, 1507–1521 (1975).
[72]C. M. Bowden and J. P. Dowling, "Near–dipole-dipole effects in dense media: Generalized Maxwell-Bloch equations," Phys. Rev. A **47**, 1247–1251 (1993).
[73]J. B. Judkins and R. W. Ziolkowski, "Finite-difference time-domain modeling of nonperfectly conducting metallic thin-film gratings," J. Opt. Soc. Am. A **12**, 1974–1983 (1995).
[74]H. F. Hofmann and O. Hess, "Quantum Maxwell-Bloch equations for spatially inhomogeneous semiconductor lasers," Phys. Rev. A **59**, 2342–2358 (1999).
[75]G. Slavcheva, J. M. Arnold, I. Wallace, and R. W. Ziolkowski, "Coupled Maxwell-pseudospin equations for investigation of self-induced transparency effects in a degenerate three-level quantum system in two dimensions: Finite-difference time-domain study," Phys. Rev. A **66**, 063418 (2002).
[76]G. M. Slavcheva, J. M. Arnold, and R. W. Ziolkowski, "FDTD simulation of the nonlinear gain dynamics in active optical waveguides and semiconductor microcavities," IEEE J. Sel. Top. Quantum Electron. **10**, 1052–1062 (2004).
[77]A. Fratalocchi, C. Conti, and G. Ruocco, "Three-dimensional *ab initio* investigation of light–matter interaction in Mie lasers," Phys. Rev. A **78**, 013806 (2008).
[78]J. Andreasen and H. Cao, "Finite-difference time-domain formulation of stochastic noise in macroscopic atomic systems," J. Lightwave Technol. **27**, 4530–4535 (2009).
[79]Strong exciton-plasmon coupling is referred to the situation where the coupling is largely relative to the separation between their resonance frequencies.
[80]M. Sukharev, T. Seideman, R. J. Gordon, A. Salomon, and Y. Prior, "Ultrafast energy transfer between molecular assemblies and surface plasmons in the strong coupling regime," ACS Nano **8**, 807–817 (2014).
[81]M. Sukharev, "Control of optical properties of hybrid materials with chirped femtosecond laser pulses under strong coupling conditions," J. Chem. Phys. **141**, 084712 (2014).
[82]M. Sukharev, P. N. Day, and R. Pachter, "Optical response of hybrid plasmon–exciton nanomaterials in the presence of overlapping resonances," ACS Photonics **2**, 935–941 (2015).
[83]A. Blake and M. Sukharev, "Surface plasmon polaritons in periodic arrays of V-shaped grooves strongly coupled to quantum emitters," Phys. Rev. B **92**, 035433 (2015).
[84]P. Törmä and W. L. Barnes, "Strong coupling between surface plasmon polaritons and emitters: A review," Rep. Prog. Phys. **78**, 013901 (2015).
[85]D. Benner, J. Boneberg, P. Nürnberger, G. Ghafoori, P. Leiderer, and E. Scheer, "Transmission of surface plasmon polaritons through atomic-size constrictions," New J. Phys. **15**, 113014 (2013).
[86]D. Benner, J. Boneberg, P. Nürnberger, R. Waitz, P. Leiderer, and E. Scheer, "Lateral and temporal dependence of the transport through an atomic gold contact under light irradiation: Signature of propagating surface plasmon polaritons," Nano Lett. **14**, 5218–5223 (2014).
[87]S. M. Sadeghi, "Quantum coherence effects in hybrid nanoparticle molecules in the presence of ultra-short dephasing times," Appl. Phys. Lett. **101**, 213102 (2012).
[88]S. Norton and T. Vo Dinh, "Spectral bounds on plasmon resonances for Ag and Au prolate and oblate nanospheroids," J. Nanophotonics **2**, 029501-1–029501-6 (2008).
[89]S. K. Gray and T. Kupka, "Propagation of light in metallic nanowire arrays: Finite-difference time-domain studies of silver cylinders," Phys. Rev. B **68**, 045415 (2003).
[90]A. E. Siegman, *Lasers* (University Science Books, Mill Valley, CA, 1986).
[91]Strictly speaking, this description is valid when spontaneous radiative decay rate can be disregarded. Otherwise the spontaneously emitted radiation is not accounted for as a source in the Maxwell equations. For this reason, we also ignore its possible dependence on position that may result from Purcell-type corrections.
[92]R. Puthumpally-Joseph, O. Atabek, M. Sukharev, and E. Charron, "Theoretical analysis of dipole-induced electromagnetic transparency," Phys. Rev. A **91**, 043835 (2015).
[93]A. Taflove and S. Hagness, *Computational Electrodynamics: The Finite-Difference Time-Domain Method*, 3rd ed. (Artech House, Boston, 2005).
[94]J. A. Roden and S. D. Gedney, "Convolution PML (CPML): An efficient FDTD implementation of the CFS–PML for arbitrary media," Microwave Opt. Technol. Lett. **27**, 334–339 (2000).
[95]L. M. Liz-Marzán, "Tailoring surface plasmons through the morphology and assembly of metal nanoparticles," Langmuir **22**, 32–41 (2006).